Pseudorotaxane formation via the slippage process with chemically cyclized oligonucleotides

Kazumitsu Onizuka[1],[*], Tomoko Chikuni[1], Takuya Amemiya[1], Takuya Miyashita[1], Kyoko Onizuka[1], Hiroshi Abe[2] and Fumi Nagatsugi[1],[*]

[1]Institute of Multidisciplinary Research for Advanced Materials, Tohoku University, 2-1-1 Katahira, Aoba-ku, Sendai, Miyagi 980-8577, Japan and [2]Department of Chemistry, Graduate School of Science, Nagoya University, Furo-cho, Chikusa-ku, Nagoya 464-8602, Japan

ABSTRACT

Circular nucleic acids have been utilized for versatile applications by taking advantage of the unique characteristic of their circular structure. In our previous study, we found that the chemically-cyclized ODN (cyODN) with double-tailed parts formed a pseudorotaxane structure with the target via the slippage process. We now report the investigation of the slippage properties and the mechanism of the slippage process using six different cyODNs. Our results indicate that the formation efficiency significantly depend on the temperature, the ring size, the target length and the mismatched position of the target. The kinetic studies also showed that this pseudorotaxane formation would proceed via a non-threaded structure which hybridizes with the target at the double-tailed parts. In addition, the resulting pseudorotaxanes showed interesting characteristics unlike the canonical duplex such as the hysteresis loop in the T_m measurements and the kinetic stabilization by lengthening the target. This information will be fundamentally important for finding new functions of circular nucleic acids and elucidating the threading mechanism regarding other synthetic small molecules and biopolymers.

INTRODUCTION

Artificial circular nucleic acids have been utilized for versatile applications such as a rolling circle amplification (1,2) or translation (3,4), decoy (5,6), siRNA (7,8), caged antisense oligo nucleotide (9–11), triplex-forming oligo nucleotide (12) and the formation of nanostructures (13–15). These applications were achieved by taking advantage of the unique characteristic of their circular structure unlike the canonical linear one. Many artificial circular nucleic

acids consist of chemically unmodified natural bases, thus, the potential of circular nucleic acids with chemical modifications is expected to find further unpredictable functions.

In our previous study, we developed the reactive oligo DNAs (ODNs) which spontaneously form a circular structure with the double-tails on the target nucleic acids for pseudorotaxane formation (Figure 1) (16). The pseudorotaxane structure was stable unlike the canonical short duplex on a denaturing polyacrylamide gel due to the unique interlocked structure. In developing the pseudorotaxane formation method, we found, by chance, that the chemically-cyclized ODN (cyODN) with double-tail parts formed the pseudorotaxane structure with the target via a slippage process (Figure 1). Interestingly, the efficiency of the pseudorotaxane formation increased with a rise in temperature and reached a peak at 50°C. However, the mechanism of the unexpected pseudorotaxane formation has remained unclear.

Generally, the formation of the pseudorotaxane structure via a slippage process using a macrocyclic ring has been studied for developing molecular machines (17) and mimics for the biopolymer process (18,19). In the study of mimics for the biopolymer process, Rowan, Notle and coworkers investigated the threading process which mimics the translocation of biopolymers using synthetic macrocycles and chains in order to understand the mechanism regarding the fundamental process, or how the threading of a long polymer through a nanometer-sized pore actually occurs (18). They suggested the threading mechanism such that the threading could be initiated and guided by weak interactions between the outside of the macrocycle and the chain. In our study of the pseudorotaxane formation with the cyODN, we validated a similar mechanism that the threading could be initiated and guided by weak interactions between the cyODN and target. Information about the unexpected pseudorotaxane formation mechanism and the properties of the synthesized cyODNs and the pseudorotaxane structures will be fundamentally important for

*To whom correspondence should be addressed. Tel: +81 22 217 5633; Fax:+81 22 217 5633; Email: nagatugi@tagen.tohoku.ac.jp
Correspondence may also be addressed to Kazumitsu Onizuka. Tel: +81 22 217 5634; Fax: +81 22 217 5633; Email: onizuka@tagen.tohoku.ac.jp
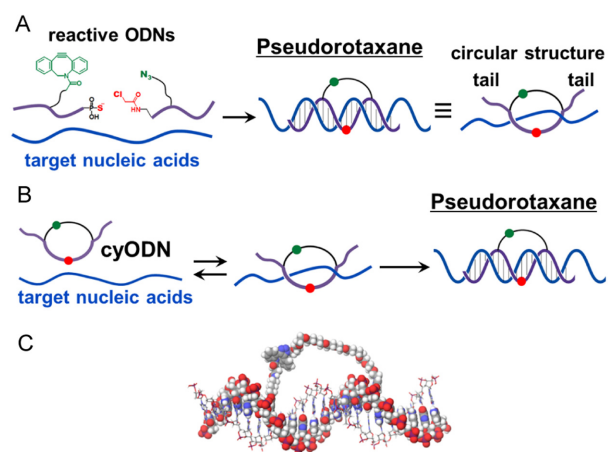
Figure 1. Schematic representation of the pseudorotaxane formation by (**A**) the chemical reactions with the reactive ODNs and (**B**) the slippage process with the cyODN. (**C**) Model of the pseudorotaxane structure calculated using the MacroModel software.

finding new functions of circular nucleic acids and designing new chemically-modified circular nucleic acids. In addition, since the intermolecular interaction between ODNs can be easily modulated just by changing the sequence and length, a systematic analysis for the slippage process is facilitated and the resulting elaborate discussion will offer a new perspective in the study of supramolecular chemistry with small organic molecules. We now report the mechanistic study of the slippage process with the cyODN and the properties of the cyODNs and the pseudorotaxane structures in order to clarify the novel character of the circular nucleic acids.

MATERIALS AND METHODS

The general chemicals were purchased from Wako Pure Chemical, Aldrich or the Tokyo Chemical Institute. The phosphoramidites and CPGs for the DNA synthesis were purchased from the Glen Research or ChemGenes Corporation. The target DNAs and RNAs were purchased from JBioS (Japan). The HPLC purification was performed by a JASCO HPLC System (PU-2089Plus, UV-2075Plus and CO-2067Plus) using a reverse-phase C$_{18}$ column (CAP-CELL PAK C18 MGII, Shiseido, 4.6 × 250 mm). MALDI-TOF MS measurements were performed by a Bruker MicrOTOFQ II instrument using a 3-hydroxypicolinic acid/diammonium hydrogen citrate matrix. The gel imaging and quantification were performed by a FLA-5100 (Fujifilm Co.).

Pseudorotaxane formation with cyODN

A solution (10 μl) of the cyclized ODN (0.5 μM) and the target (0.25 μM) in phosphate buffer (20 mM, pH 7.2) containing NaCl (100 mM) was incubated at 20, 37 or 50°C. The aliquots (1.4 μl each) were removed from the reaction mixture at various time points, quenched by a loading buffer (80% formamide, 10 mM ethylenediaminetetraacetic acid (EDTA), 1.4 μl), then rapidly cooled to 0°C. Electrophoresis was performed at 15°C on a 20% denaturing polyacry-

lamide gel with 1 × Tris-borate-EDTA (TBE) and 7.5 M urea at 200 V for 1 h.

Pseudorotaxane formation to the mismatched target ODN

A solution (10 μl) of cyclized ODN (0.25 μM) and the target (0.25 μM) in phosphate buffer (20 mM, pH 7.2) containing NaCl (100 mM) was incubated at 20, 25, 31 or 37°C. The aliquots (1.4 μl each) were removed from the reaction mixture at various time points and quenched by loading buffer (40% glycerol, 5 mM EDTA, 2.6 μl), then rapidly cooled to 0°C. Electrophoresis was performed at 15°C on a 20% native polyacrylamide gel with 1 × TBE at 200 V for 1 h. The second-order rate constant of the pseudorotaxane formation (k_{on}) was graphically obtained from the second-order kinetic plot (Equation 1). The k_{on} values were determined from two or three separate experiments. The obtained rate constants (k_{on}) were subjected to the Eyring plot and the values of $\Delta H_{on}^{\ddagger}$ and $\Delta S_{on}^{\ddagger}$ were graphically obtained by Equation (2). The value of $\Delta G_{on}^{\ddagger}$ was obtained by Equation (3).

$$1/[\text{pseudorotaxane}]_t = 1/[\text{pseudorotaxane}]_0 + k_{on} \cdot t \quad (1)$$

$$\ln(k/T) = \ln(k_B/h) - \Delta H_{on}^{\ddagger}/RT + \Delta S_{on}^{\ddagger}/R \quad (2)$$

k_B: Boltzmann constant, $k_B = 1.381 \times 10^{-23}$ J·K^{-1}, h: Planck constant, $h = 6.626 \times 10^{-34}$ J·s and R: gas constant, $R = 8.314$ J K^{-1} mol^{-1}.

$$\Delta G_{on}^{\ddagger} = \Delta H_{on}^{\ddagger} - T\Delta S_{on}^{\ddagger} \quad (3)$$

Melting temperature (T_m) measurement

A mixture of the cyODN (0.1 μM) and template (0.1 μM) in phosphate buffer (20 mM, pH 7.2) containing NaCl (100 mM) was transferred to a microquartz cell with a 1-cm path length. The melting temperature was then measured under UV absorption at 260 nm from 25°C to 95°C at the rate of 1°C/min. The first measurement was carried out to form the pseudorotaxane structure instead of annealing. The measurements were then carried out three times per each sample and averaged for obtaining the final value. The melting temperature measurement was performed by a DU-800 (Beckman-coulter) equipped with a temperature controller.

Determination of dissociation rate constants (k_{off}) of cyODNs

A solution (6.25 μl) of the cyclized ODN (0.6 μM) and the target (0.4 μM) in phosphate buffer (20 mM, pH 7.2) containing NaCl (100 mM) was incubated at 50°C for 15 min (28 mer) or 3 h (60 mer) to form the pseudorotaxane structure. The mixture was then diluted with a solution (18.75 μl) of the non-labeled ODN**14** or ORN**3** target in phosphate buffer containing NaCl. The diluted solution (25 μl) of the pseudorotaxane (0.1 μM) and non-labeled target (2 μM) was incubated at various temperatures. Aliquots (2.5 μl each) were removed from the reaction mixture at various time points and quenched by loading buffer (80% formamide, 10 mM EDTA, 2.5 μl), then rapidly cooled to 0°C.

Electrophoresis was performed at 15°C on a 20% denaturing polyacrylamide gel with $1 \times$ TBE at 200 V for 1 h. The first-order rate constant of the dissociation (k_{off}) was graphically obtained from the first-order kinetic plot (Equation 4). The k_{off} values were determined from two or three separate experiments. The obtained rate constants (k_{off}) were subjected to the Eyring plot and the values of $\Delta H_{off}^{\ddagger}$ and $\Delta S_{off}^{\ddagger}$ were obtained by Equation (2). The value of $\Delta G_{off}^{\ddagger}$ was obtained by Equation (3).

$$\ln[\text{pseudorotaxane}]_t = \ln[\text{pseudorotaxane}]_0 - k_{off} \cdot t \quad (4)$$

Thermo-reversible pseudorotaxane formation

Aliquots (2 μl) of the cyclized ODN (0.5 μM) and the target (0.25 μM) in phosphate buffer (20 mM, pH 7.2) containing NaCl (100 mM) were incubated at 50°C for 5 min in the formation step and at 80°C for 5 min in the dissociation step. The aliquot was quenched at each step by a stop buffer (80% formamide, 10 mM EDTA, 1.3 μM non-labeled target ODN**14**, 4 μl), then rapidly cooled to 0°C. Electrophoresis was performed at 15°C on a 20% denaturing polyacrylamide gel with $1 \times$ TBE and 7.5 M urea at 200 V for 1 h.

RESULTS AND DISCUSSION

Molecular design and synthesis of cyODNs

The ODN and ORN sequences and the structures of the modified nucleotides used in this study for the synthesis of the cyODNs and the slippage formation are shown in Table 1 and Figure 2. The sequence and structure of the cyODNs are shown in Figure 3. Six different cyODNs with different modified nucleotides and modified positions were designed in order to systematically investigate the slippage properties of the cyODN. Base-10, 11 and 13 consist of base-modified nucleotides for the cyclization, and sugar-10, 11 and 13 consist of sugar-modified nucleotides. The number indicates the base number of the cyclic part and the ring size of the cyODN increases as the number is increased. Generally, the base-modified type cyODN has a linker on the major groove, in contrast, the sugar-modified type cyODN has a linker on the minor groove. We expected that systematically investigating the pseudorotaxane formation rate of the cyODNs with the different linkage positions and ring sizes will provide valuable information to discuss the slippage mechanism and find new functions of the cyODN.

The cyODNs were synthesized with ODN**1**, **2** or **3** (R^1 = BCN) and ODN**4** (Y = T, N_3 linker, Z = T, IAc) under dilute conditions and purified by gel electrophoresis followed by HPLC (Supplementary Scheme S1). Two reactions, the copper-free click reaction and S_N2 reaction, occurred to provide a cyODN as the major product. The products were confirmed by MALDI-TOF mass spectroscopy (Supplementary Table S1). The bicyclo[6.1.0]nonyne (BCN) derivative (20) was used for the copper-free click reaction to produce a single regioisomer upon cycloaddition instead of the dibenzylcyclooctyne derivative we previously used (16).

Pseudorotaxane formation with cyODN

The pseudorotaxane formations via the slippage process were performed with the cyODN and the 28 or 60 mer target DNA at three different temperatures (20°C, 37°C or 50°C) (Figure 4). The formations were analyzed by denaturing polyacrylamide gel electrophoresis (PAGE). The gel image of the pseudorotaxane formation with cyODN(sugar-11) and 28 mer ODN**5** at 37°C is shown in Figure 4A. One new clear band indicating the pseudorotaxane structure was observed and the target was almost consumed in 60 min. The time course experiments at the different temperatures showed that the formation efficiency significantly increased with a rise in temperature. The efficiency with the 60 mer target ODN was much lower than that with the 28 mer target ODN. These results indicated that this slippage process requires energy to thread the cyclic part of the cyODN, thus the longer target requires much more energy than the shorter target. As for the ring size, the cyODN with the higher base number on the cyclic part showed a higher efficiency (13 > 11 > 10). Especially, cyODN(sugar-13) showed an remarkably high efficiency and the formation yield reached over 80% within 15 min even at 20°C (Figure 4J). On the other hand, cyODN(base-10) or cyODN(sugar-10) was definitely dependent on the temperature, that is to say, the formation did not proceed at 20°C, while the efficient formation was seen at 50°C (Figure 4B and H). This is a unique property of the cyODN because canonical nucleic acids usually form a duplex at a lower temperature rather than at a higher one. As for the RNA target, all of the pseudorotaxane formations showed similar temperature and target length dependencies to the DNA target (Supplementary Figure S1). In addition, the second-order rate constants (k_{on}) of the pseudorotaxane formation at 37°C were calculated (Table 2). CyODN(sugar-13) showed a significantly high formation rate compared to the other cyODNs and it was 120 or 30 times higher than the rate of cyODN(sugar-10) to the DNA or RNA target, respectively. One of the reasons for this remarkable high formation rate is that cyODN(sugar-13) has a larger cyclic part than cyODN(sugar-10). However, the mechanistic reasons still remained unclear based on these results.

Mechanistic study of pseudorotaxane formation using mismatched target ODN

The pseudorotaxane formations using the mismatched target ODN were carried out at 37°C in order to discuss the mechanism of the slippage process and the reason for the difference in the formation rate among the cyODNs. The formations were analyzed by native PAGE because the cyODN dissociated from the mismatched target on the denaturing PAGE. Based on the sequence of the full match target ODN**5**, we incorporated the mismatched part, TT or T, into the middle (ODN**7**), 3′-side (ODN**8**), 5′-side (ODN**9**) and both the 3′ and 5′-sides (ODN**10**) (Figure 5). The second-order rate constants (k_{on}) of the pseudorotaxane formations to the mismatched target ODN are shown in Table 3. When the mismatched part was at the middle, the formation rate was almost the same as the full matched one (the ratio to full matched one: 0.96–1.1). In contrast, when at the 3′ or
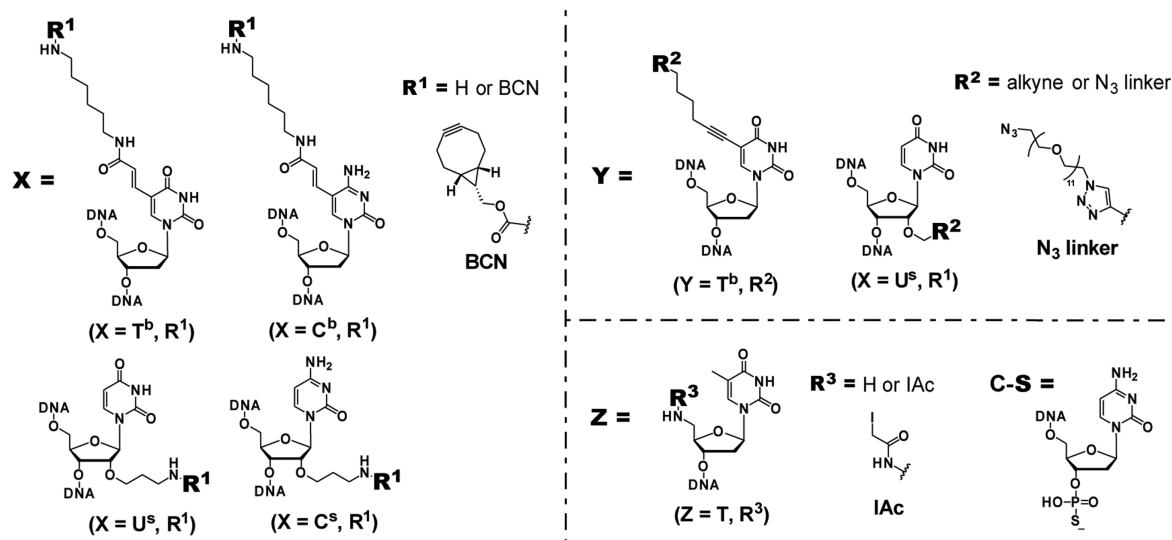
Figure 2. Structures of modified nucleotide.
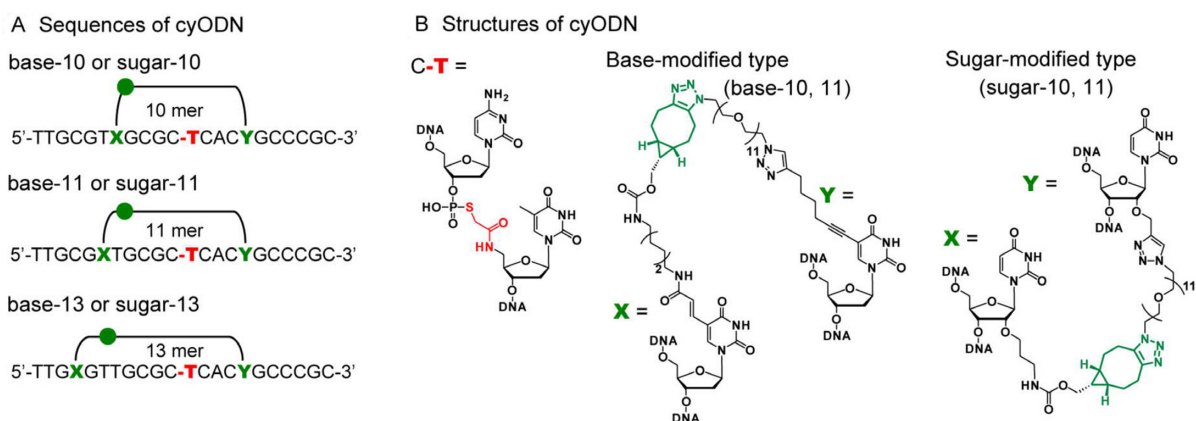
Figure 3. (**A**) Sequences and (**B**) structures of cyODN.

Table 1. ODN and ORN sequences used in this study

Entry	Sequences (5′-3′)
ODN1	TTGCGT**X**GCGC-S (**X** = T^b or U^s, R^1)
ODN2	TTGCG**X**TGCGC-S (**X** = T^b or U^s, R^1)
ODN3	TTG**X**GTTGCGC-S (**X** = C^b or C^s, R^1)
ODN4	**Z**CAC**Y**GCCCGC (**Y** = T^b or U^s, R^2, **Z** = T, R^3)
ODN5	FAM-AAAGCGGGCAGTGAGCGCAACGCAATTA
ODN6	FAM-TTTTAGCTAGCTAGCTAAAGCGGGCAGTGAGCGCAACGCAATTAAGCTAGCTAGCTTTTT
ODN7	FAM-AAAGCGGGCAGTGTTCGCAACGCAATTA
ODN8	FAM-AAAGCGGGCAGTGAGCGCAACTTAATTA
ODN9	FAM-AAAGCTTGCAGTGAGCGCAACGCAATTA
ODN10	FAM-AAAGCTTGCAGTGAGCGCAACGTAATTA
ODN11	FAM-TTTTTTTTAGCTAGCTAGCTAGCTAGCTAGCTAAAGCGGGCAGTGAGCGCAACGCAATTA
ODN12	FAM-AAAGCGGGCAGTGAGCGCAACGCAATTAAGCTAGCTAGCTAGCTAGCTAGCTTTTTTTTTT
ODN13	TTGCGTTGCGCTCACTGCCCGC
ODN14	GCGGGCAGTGAGCGCAACGCAA
ORN1	FAM-AAAGCGGGCAGUGAGCGCAACGCAAUUA
ORN2	FAM-UUUUAGCUAGCUAGCUAAAGCGGGCAGUGAGCGCAACGCAAUUAAGCUAGCUAGCUUUUU
ORN3	GCGGGCAGUGAGCGCAACGCAA
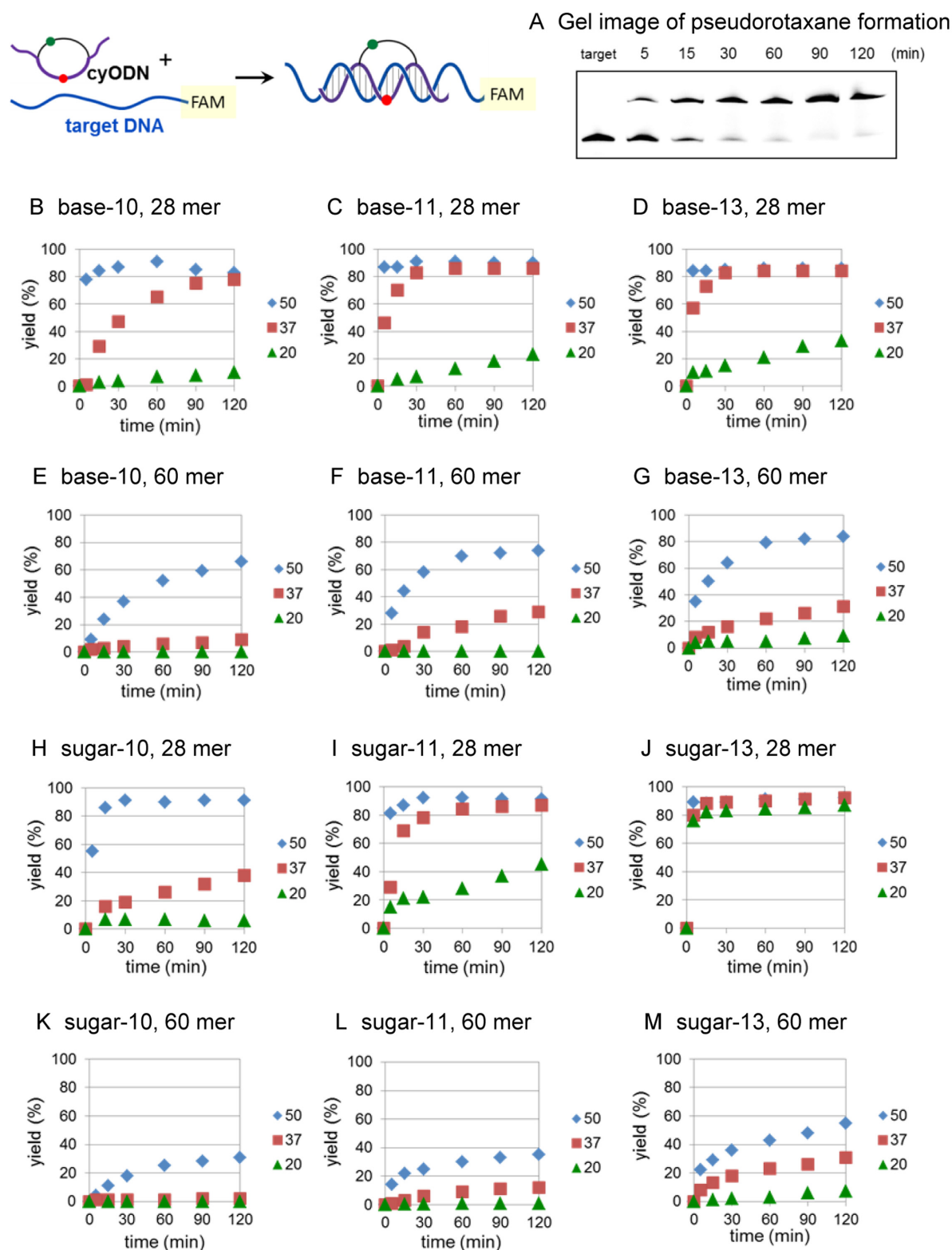
Figure 4. Pseudorotaxane formation using cyODN and DNA target. The formation was carried out with cyODN (0.5 μM) and target ODN5 or ODN6 (0.25 μM) in phosphate buffer (20 mM, pH 7.2) containing NaCl (100 mM) at 20, 37 or 50°C. (**A**) Gel image of pseudorotaxane formation using cyODN(sugar-11) and 28 mer ODN5 at 37°C. The electrophoresis was performed at 15°C on a 20% denaturing polyacrylamide gel. (**B**) cyODN(base-10) and 28 mer ODN5. (**C**) cyODN(base-11) and 28 mer ODN5. (**D**) cyODN(base-13) and 28 mer ODN5. (**E**) cyODN(base-10) and 60 mer ODN6. (**F**) cyODN(base-11) and 60 mer ODN6. (**G**) cyODN(base-13) and 60 mer ODN6. (**H**) cyODN(sugar-10) and 28 mer ODN5. (**I**) cyODN(sugar-11) and 28 mer ODN5. (**J**) cyODN(sugar-13) and 28 mer ODN5. (**K**) cyODN(sugar-10) and 60 mer ODN6. (**L**) cyODN(sugar-11) and 60 mer ODN6. (**M**) cyODN(sugar-13) and 60 mer ODN6.

Table 2. Second-order rate constants (k_{on}) of pseudorotaxane formation

cyODN	Target	k_{on} [M^{-1}s^{-1}][a]	Ratio[b]
Base-10	ODN5	8.7×10^2	-
Base-11	ODN5	3.0×10^3	3.4
Base-13	ODN5	8.2×10^3	9.4
Sugar-10	ODN5	2.0×10^2	-
Sugar-11	ODN5	5.3×10^3	27
Sugar-13	ODN5	2.4×10^4	120
Base-10	ORN1	7.4×10	-
Base-11	ORN1	4.1×10^2	5.5
Base-13	ORN1	1.9×10^3	26
Sugar-10	ORN1	2.2×10^2	-
Sugar-11	ORN1	8.9×10^2	3.9
Sugar-13	ORN1	6.6×10^3	30

[a]Estimated error <25%.
[b]Ratio = k_{on}(cyODN-11 or -13)/k_{on}(cyODN-10).
The formation was carried out with cyODN (0.25 μM) and target ODN5 or ORN1 (0.25 μM) in phosphate buffer (20 mM, pH 7.2) containing NaCl (100 mM) at 37°C.

```
cyODN(11): 5'-TTGCGXTGCGC-TCACYGCCCGC-3'
cyODN(13): 5'-TTGXGTTGCGC-TCACYGCCCGC-3'

ODN5(full):   3'-ATTAACGCAACGCGAGTGACGGGCGAAA-FAM-5'
ODN7(mid):    3'-ATTAACGCAACGCTTGTGACGGGCGAAA-FAM-5'
ODN8(3'):     3'-ATTAATTCAACGCGAGTGACGGGCGAAA-FAM-5'
ODN9(5'):     3'-ATTAACGCAACGCGAGTGACGTTCGAAA-FAM-5'
ODN10(3'5'):  3'-ATTAATGCAACGCGAGTGACGTTCGAAA-FAM-5'
```

Figure 5. Mismatch sequences for mechanistic study. Bold T except in cyODN shows mismatched T and the background color indicates the hybridization possible regions.

5′-side, the formation rate decreased (3′-side: 0.39–0.63, 5′-side: 0.11–0.34). Moreover, the mismatch at both the 3′ and 5′-sides made the formation rate much lower than the others (0.026–0.094). These results indicate that the double-tailed parts of the cyODN play significant role in the pseudorotaxane formation.

To obtain further insight into the effect of the double-tailed part, the pseudorotaxane formation was carried out with the mismatched target at different temperatures (20, 25, 31 and 37°C). The kinetic parameters were calculated using the Eyring equation (Supplementary Figure S2) and are shown in Table 4. It should be noted that the entropy of activation ($\Delta S_{on}^{\ddagger}$) was a positive value despite the intermolecular formation which is normally a negative value (18,19,21), suggesting that this pseudorotaxane formation will be initiated and guided by the formation of an intermediate complex (22). Given that the double-tailed parts of cyODN played a significant role in the pseudorotaxane formation, the pseudorotaxane formation will form a non-threaded structure which hybridizes with the target at the double-tailed parts of the cyODN as the intermediate complex. The proposed mechanism of the pseudorotaxane formation with cyODN is shown in Figure 6. This slippage formation can be divided into two steps; one is a pre-equilibrium step, and the other is a threading step. The

intermediate formation in the pre-equilibrium step would guide the threading by efficiently approaching the ring part to the end of the target. When the pre-equilibrium constant represents K (= k_1/k_{-1}), the threading rate represents k_2 and k_2', and k_2, k_2' ≪ k_1, k_{-1} is assumed, the pseudorotaxane formation rate constant (k_{on}) can be generally depicted by Equation (5) (23).

$$k_{on} = K(k_2 + k_2') \qquad (5)$$

When the cyODN forms the non-threaded structure with the target DNA or RNA in the pre-equilibrium step, the pre-equilibrium constant K depends on the stability of the double-tailed parts. Thus, the step will be accelerated by the strong hybridization with the double-tailed parts. The threading process then proceeds by the dissociation of one tail part from the non-threaded structure to produce the threaded structure. In this threading step, the stability of each tail part will also affect the threading rate (k_2 and k_2') because the dissociation of one tail part is required. Contrary to the pre-equilibrium step, the threading step will be decelerated by the strong hybridization with the double-tailed parts. Overall, an adequate stability of the non-threading structure is required for the efficient formation. In fact, in Table 4, both the $\Delta S_{on}^{\ddagger}$ and the enthalpy of activation ($\Delta H_{on}^{\ddagger}$) increased with an increase in the matching base pair numbers of the double-tailed parts, indicating that the slippage of the cyODN becomes entropically favorable and enthalpically unfavorable as the non-threading structure becomes stable. This suggests that the stabilization of the double-tailed parts favorably affected the pre-equilibrium step from the increase in $\Delta S_{on}^{\ddagger}$ which will mainly mean the stability of the non-threading structure, but unfavorably affected the threading step from the increase in $\Delta H_{on}^{\ddagger}$ which will mainly mean the energy to dissociate one tail part. These results clearly support the proposed mechanism.

Based on the proposed mechanism, we can successfully discuss the reason for the difference in the formation rate. As for cyODN(base-13) or cyODN(sugar-13), the stabil-

Table 3. Second-order rate constants (k_{on}) of pseudorotaxane formation

cyODN	Target	TT	k_{on} [M^{-1}s^{-1}][a]	Ratio[b]
Base-11	ODN5	-	7.7×10^3	-
Base-11	ODN7	Mid	8.0×10^3	1.0
Base-11	ODN8	3′	3.0×10^3	0.39
Base-11	ODN9	5′	1.2×10^3	0.16
Base-11	ODN10	3′5′	6.2×10^2	0.081
Base-13	ODN5	-	1.6×10^4	-
Base-13	ODN7	Mid	1.7×10^4	1.1
Base-13	ODN8	3′	1.0×10^4	0.63
Base-13	ODN9	5′	3.8×10^3	0.24
Base-13	ODN10	3′5′	1.5×10^3	0.094
Sugar-11	ODN5	-	8.5×10^3	-
Sugar-11	ODN7	Mid	8.1×10^3	1.0
Sugar-11	ODN8	3′	3.9×10^3	0.46
Sugar-11	ODN9	5′	2.9×10^3	0.34
Sugar-11	ODN10	3′5′	2.4×10^2	0.028
Sugar-13	ODN5	-	4.6×10^4	-
Sugar-13	ODN7	Mid	4.4×10^4	0.96
Sugar-13	ODN8	3′	2.8×10^4	0.61
Sugar-13	ODN9	5′	5.0×10^3	0.11
Sugar-13	ODN10	3′5′	1.2×10^3	0.026

[a] Estimated error <15%.
[b] Ratio = k_{on}(mismatch)/k_{on}(full match).
The formation was carried out with cyODN (0.25 μM) and target ODN (0.25 μM) in phosphate buffer (20 mM, pH 7.2) containing NaCl (100 mM) at 37°C.
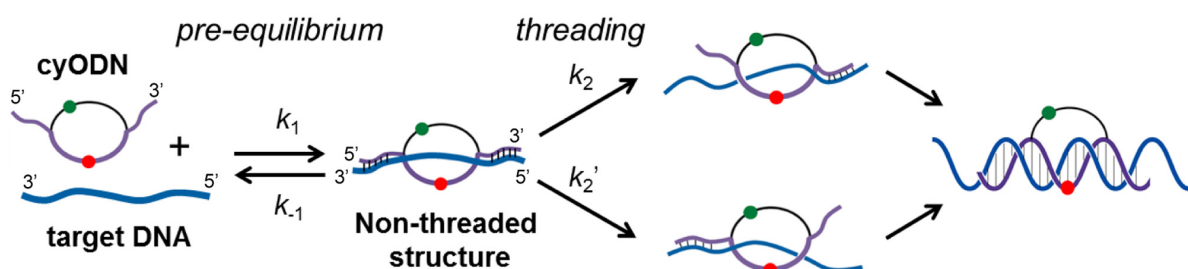
Figure 6. Proposed mechanism of pseudorotaxane formation by the slippage process with cyODN.

Table 4. Second-order rate constants (k_{on}) and the activation parameters for the slippage process

cyODN	target	TT	k_{on} [M^{-1}s^{-1}](37°C)	$\Delta G_{on}^{\ddagger}$ [kJmol^{-1}](37°C)	$\Delta H_{on}^{\ddagger}$ [kJmol^{-1}]	$\Delta S_{on}^{\ddagger}$ [Jmol^{-1}K^{-1}]
Base-11	ODN5	-	7.7×10^3	53	1.9×10^2	4.4×10^2
Base-13	ODN5	-	1.6×10^4	51	1.8×10^2	4.2×10^2
Base-13	ODN8	3′	1.0×10^4	52	1.7×10^2	3.8×10^2
Base-13	ODN9	5′	3.8×10^3	55	1.5×10^2	3.0×10^2
Sugar-11	ODN5	-	8.5×10^3	53	1.7×10^2	3.9×10^2
Sugar-13	ODN5	-	4.6×10^4	48	1.6×10^2	3.5×10^2
Sugar-13	ODN8	3′	2.8×10^4	49	1.5×10^2	3.3×10^2
Sugar-13	ODN9	5′	5.0×10^3	54	8.9×10	1.1×10^2

ity of the double-tailed parts is not balanced. According to the DNA/DNA nearest-neighbor parameters, the $\Delta G°_{37}$ values of the cyODN(13)-5′ side (TTGC/GCAA) and cyODN(13)-3′ side (TGCCCGC/GCGGGCA) are −7.5 kJ mol^{-1} and −41.4 kJ mol^{-1}, respectively (Supplementary Table S2) (24). This stability imbalance between the double-tailed parts (5′ side: −7.5 kJ mol^{-1} versus 3′ side:

−41.4 kJ mol^{-1}) will contribute to the remarkably high formation rate because one short tailed part is easily dissociated from the non-threaded structure. In addition, the threading direction can be controlled because the k_2 value will be much higher than the k_2' value due to the stability imbalance (Figure 6). On the other hand, the $\Delta G°_{37}$ value of the cyODN(11)-5′ side (TTGCGT/ACGCAA) is

-25.5 kJ mol^{-1} (Supplementary Table S2). Since the difference between the double-tailed parts of cyODN(11) (5′ side: -25.5 kJ mol^{-1} versus 3′ side: -41.4 kJ mol^{-1}) is smaller than that of cyODN(13), the formation rate of cyODN(11) would be lower. The difference between the k_2 and k_2' values of cyODN(11) will also be much smaller than that of cyODN(13). As for the formation rate to the mismatched target, the 3′-mismatched target ODN**8** had a higher formation rate than the 5′-mismatched target ODN**9** because one stronger tail binding was maintained when using the 3′-mismatched target ODN**8** while the non-threaded structure stability of cyODN(13)-ODN**9** would be insufficient for the efficient formation. Especially, the insufficient stability of the cyODN(sugar-13)-ODN**9** is supported by the drastic decrease in both $\Delta H_{\mathrm{on}}^{\ddagger}$ and $\Delta S_{\mathrm{on}}^{\ddagger}$.

Mechanistic study of pseudorotaxane formation using longer target ODN

In order to validate our proposed mechanism, the pseudorotaxane formations using the longer 60 mer target ODN were carried out at 37°C. Based on ODN**6** with the 19 mer non-target site at both ends, we designed ODN**11** and ODN**12** with the 35 mer non-target site at the 5′-end or at the 3′-end, respectively (Figure 7). The second-order rate constants of the pseudorotaxane formation using the 60 mer target ODN are shown in Table 5. The formation rates to ODN**11** with the same 3′-end as the 28 mer ODN**5** were much faster than the others and were close to the formation rates of the 28 mer ODN**5** (Tables 2 and 5). The formation rates to ODN**11** were 37–93 times faster than those to ODN**6** with the non-target site at both ends due to the longer slippage distance (Figure 7A and B). The formation rates to ODN**12** decreased by 10–50% compared to ODN**11** but were still 4–18 times faster than those to ODN**6**, suggesting that the slippage to ODN**12** mainly occurred from the 5′-end of the target by the hybridization at the 5′-end of the cyODN (Figure 7C). These results are in accord with the mismatched target experiments and clearly indicate that the double-tailed parts of cyODN play a significant important role in the formation rate and direction of the pseudorotaxane formation, and this pseudorotaxane formation selectively proceeded to the terminal target sequence.

Stability of the pseudorotaxane structures

The thermal and kinetic stability of the pseudorotaxane structures were investigated in order to understand the characteristics of each structure. Melting temperature (T_{m}) measurements were first performed to provide an insight into the thermal stability of the pseudorotaxane structures and the T_{m} values are shown in Table 6. As for the DNA–DNA pseudorotaxane structure, the T_{m} values decreased by 5.6–11.8°C compared to the canonical ODN**13**–ODN**5** duplex. For the DNA–RNA pseudorotaxane structure, the T_{m} values with the base-modified cyODN also decreased by 6.1–7.9°C while the T_{m} values with the sugar-modified cyODN underwent a slight decrease by 0.1–1.8°C. The T_{m} values with cyODN(base) may decrease by the disturbance in the duplex structure resulting from the direct linkage of the nucleobases which is important for the molecular recognition.

In contrast, for cyODN(sugar), the sugar part would be a buffer, and the linker would not significantly disturb the duplex structure. However, since the 2'-modification is generally unfavorable for the DNA–DNA duplex, the T_{m} value of the cyODN(sugar)-DNA pseudorotaxanes was lower than that of the cyODN(sugar)-RNA pseudorotaxanes. Interestingly, the forward and reverse T_{m} values with the cyODNs were significantly different, especially, the difference was 12°C with the cyODN(sugar-10) (F-R in Table 6). The forward and reverse T_{m} curves with cyODN(sugar-10)-ODN**5** and ODN**13**–ODN**5** are shown in Figure 8. A hysteresis loop was observed using cyODN(sugar-10)-ODN**5** because of the slow rate of the pseudorotaxane formation and the lower T_{m} value of the double-tailed part than that of the full strand. In contrast, the hysteresis loop was not observed using ODN**13**–ODN**5** (Figure 8B). The difference between the forward and reverse T_{m} values well represents the intriguing characteristic of the pseudorotaxane structure.

Next, the kinetic stability was investigated by the determination of the dissociation rate constants (k_{off}) of the cyODNs and the half-life ($t_{1/2}$) of the pseudorotaxanes in the dethreading reaction. The pseudorotaxane structure was formed at 50°C and the cyODN was dethreaded at 60°C for the DNA–DNA pseudorotaxane or 67.5°C for the DNA–RNA one, and the dethreaded cyODN was trapped with the non-labeled target ODN**14** or ORN**3**. From a gel shift assay, the first-order rate constant of the dethreading and its half-life were calculated (Figure 9). The dissociation rate constants and its half-lives using the 28 mer and 60 mer targets are shown in Table 7 for the DNA target and Table 8A for the RNA target. The dissociation rate constant of cyODN(base-13) from the RNA target could not be inexplicably calculated as a first-order reaction rate constant. The half-life of the pseudorotaxane with a smaller ring size was longer; $t_{1/2}(10) > (11) > (13)$. When the longer target 60 mer ODN or ORN was used, the half-life got longer than the 28 mer target because the distance between the target and the end got longer. The difference between $t_{1/2}$(60mer) and $t_{1/2}$(28mer) also got greater using the cyODN with the smaller ring size. Given that the difference between the $t_{1/2}$(60mer) and $t_{1/2}$(28mer) using the canonical duplex (5–6 min, Table 8C) was much smaller than that using cyODN (17–67 min, Table 8A and B), these kinetic stabilizations of the complex also represent the unique character of the pseudorotaxane structure. Due to this kinetic stabilization, the pseudorotaxanes with cyODN(sugar)-RNA were kinetically more stable than that with the canonical duplex even though the T_{m} values slightly decreased.

To obtain a further insight into the kinetic stabilization by the pseudorotaxane formation, the temperature dependence of the dissociation rate constants was investigated (Supplementary Figure S3). The kinetic parameters were calculated using the Eyring equation (Supplementary Figure S4) and are shown in Tables 9 and 10. It is expected that the entropic effect contributes to the kinetic stabilization of the cyODN with the small ring; that is, the structure changes in the pseudorotaxane with the smaller ring in the transition state will be restricted and the entropy of activation ($\Delta S_{\mathrm{off}}^{\ddagger}$) will be lower whereas the enthalpy of activation ($\Delta H_{\mathrm{off}}^{\ddagger}$) remains constant. As for the pseudorotaxane of cyODN(base)-ODN and cyODN(sugar)-

cyODN(11): 5'-TTGCG**X**TGCGC-**T**CAC**Y**GCCCGC-3'
cyODN(13): 5'-TTG**X**GTTGCGC-**T**CAC**Y**GCCCGC-3'

ODN6(3'5'): 3'-TTTTTCGATCGATCGAATT**AACGC**AACGCGAGT**GACGGGCG**AAATCGATCGATCGATTTT-FAM-5'
ODN11(5'): 3'-ATT**AACGC**AACGCGAGT**GACGGGCG**AAATCGATCGATCGATCGATCGATCGATTTTTTTT-FAM-5'
ODN12(3'): 3'-TTTTTTTTTCGATCGATCGATCGATCGATCGAATT**AACGC**AACGCGAGT**GACGGGCG**AAA-FAM-5'
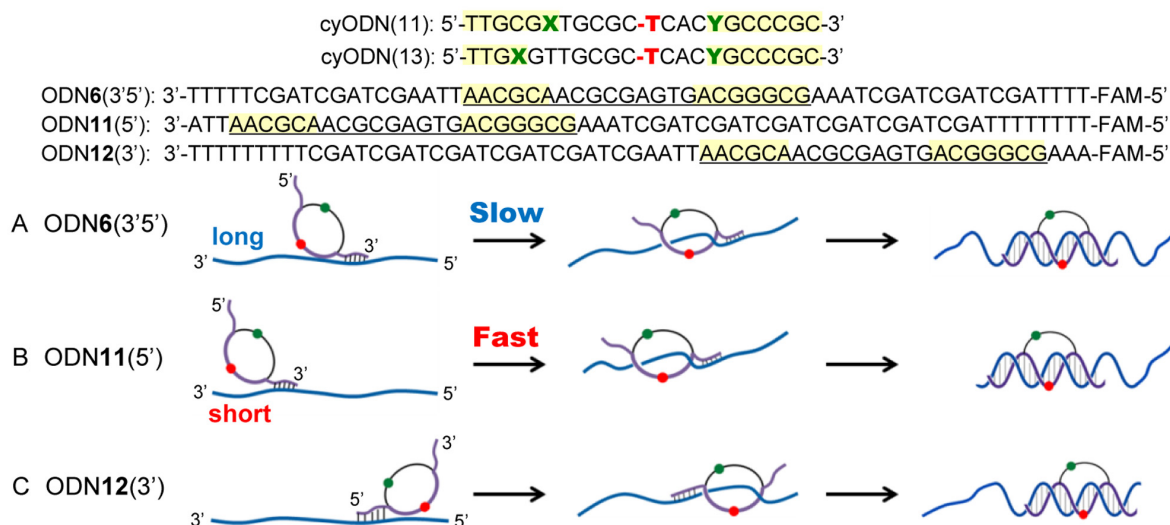
Figure 7. Long DNA (60 mer) sequences and the proposed slippage mechanism. The background color indicates the possible hybridization regions.

Table 5. Second-order rate constants (k_{on}) of pseudorotaxane formation with long target ODN

cyODN	target	k_{on} [M^{-1}s^{-1}][a]	ratio[b]
Base-11	ODN6	8.1×10	-
Base-11	ODN11	3.2×10^3	40
Base-11	ODN12	3.2×10^2	4.0
Sugar-11	ODN6	1.1×10^2	-
Sugar-11	ODN11	5.0×10^3	44
Sugar-11	ODN12	4.3×10^2	3.8
Base-13	ODN6	3.3×10^2	-
Base-13	ODN11	1.2×10^4	37
Base-13	ODN12	6.0×10^3	18
Sugar-13	ODN6	4.2×10^2	-
Sugar-13	ODN11	3.9×10^4	93
Sugar-13	ODN12	5.2×10^3	12

[a] Estimated error <20% for **ODN11** and **12**, <45% for **ODN6**.
[b] Ratio = k_{on}(ODN11 or 12)/k_{on}(ODN6).
The formation was carried out with cyODN (0.25 μM) and target ODN (0.25 μM) in phosphate buffer (20 mM, pH 7.2) containing NaCl (100 mM) at 37°C.

Table 6. T_m values of pseudorotaxane structure

cyODN	Target	T_m (°C)	ΔT_m	Reverse	F-R[a]
ODN13	ODN5	74.9	-	73.3	1.6
Base-10	ODN5	66.7	−8.2	62.9	3.8
Base-11	ODN5	68.0	−6.9	62.7	5.3
Base-13	ODN5	65.7	−9.2	64.8	0.9
Sugar-10	ODN5	69.3	−5.6	57.2	12.1
Sugar-11	ODN5	68.9	−6.0	57.2	11.7
Sugar-13	ODN5	63.1	−11.8	59.2	3.9
ODN13	ORN1	75.7	-	74.3	1.4
Base-10	ORN1	67.8	−7.9	64.5	3.3
Base-11	ORN1	69.2	−6.5	67.1	2.1
Base-13	ORN1	69.6	−6.1	68.0	1.6
Sugar-10	ORN1	75.6	−0.1	63.4	12.2
Sugar-11	ORN1	73.9	−1.8	64.2	9.7
Sugar-13	ORN1	74.6	−1.1	68.2	6.4

[a] Forward T_m – Reverse T_m.
The T_m values were measured using cyODN (0.1 μM) and target ODN (0.1 μM) in phosphate buffer (20 mM, pH 7.2) containing NaCl (100 mM).

Table 7. Dissociation rate constants (k_{off}) of cyODN from DNA target ODN5 or ODN6 at 60°C

cyODN	k_{off} (s^{-1})^a (28 mer)	k_{off} (s^{-1})^a (60 mer)	$t_{1/2}$ (min) (28 mer)	$t_{1/2}$ (min) (60 mer)	$t_{1/2}$(60 mer)-$t_{1/2}$(28 mer) (min)
Base-10	8.0×10^{-4}	6.3×10^{-5}	14	185	171
Base-11	1.5×10^{-3}	1.7×10^{-4}	7.9	69	61
Base-13	2.2×10^{-3}	1.4×10^{-3}	5.4	8.1	2.7
Sugar-10	7.3×10^{-5}	2.6×10^{-5}	158	439	281
Ssugar-11	2.3×10^{-4}	5.0×10^{-5}	51	233	182
Sugar-13	1.2×10^{-3}	4.7×10^{-4}	9.6	24	14

^{a}Estimated error <25%.

Table 8. Dissociation rate constants (k_{off}) of cyODN from (A) RNA target or (B) DNA target at 67.5°C

	cyODN	Target	k_{off} (s^{-1})^a (28 mer)	k_{off} (s^{-1})^b (60 mer)	$t_{1/2}$ (min) (28 mer)	$t_{1/2}$ (min) (60 mer)	$t_{1/2}$(60 mer)-$t_{1/2}$(28 mer) (min)
A (RNA)	Base-10	**ORN1** or **ORN2**	1.1×10^{-2}	5.7×10^{-4}	1.1	20	19
	Base-11	**ORN1** or **ORN2**	1.3×10^{-2}	$6.3 \times 10^{-4\,c}$	0.9	18	17
	Sugar-10	**ORN1** or **ORN2**	$1.4 \times 10^{-4\,\ddagger}$	$7.7 \times 10^{-5\,c}$	83	150	67
	Sugar-11	**ORN1** or **ORN2**	2.0×10^{-4}	1.1×10^{-4}	59	109	50
	Sugar-13	**ORN1** or **ORN2**	1.9×10^{-4}	1.3×10^{-4}	62	89	27
B (DNA)	Base-10	**ODN5** or **ODN6**	1.1×10^{-2}	5.0×10^{-4}	1.1	23	22
	Sugar-10	**ODN5** or **ODN6**	2.1×10^{-3}	3.1×10^{-4}	5.6	37	32
C (canonical)	**ODN13**	**ODN5** or **ODN6**	4.0×10^{-4}	3.4×10^{-4}	29	34	5
	ODN13	**ORN1** or **ORN2**	4.2×10^{-4}	3.4×10^{-4}	28	34	6

^{a}Estimated error <15%.
^{b}Estimated error <15%.
^{c}Estimated error <30%.
(C) Dissociation rates (k_{off}) of canonical duplex at 67.5°C.
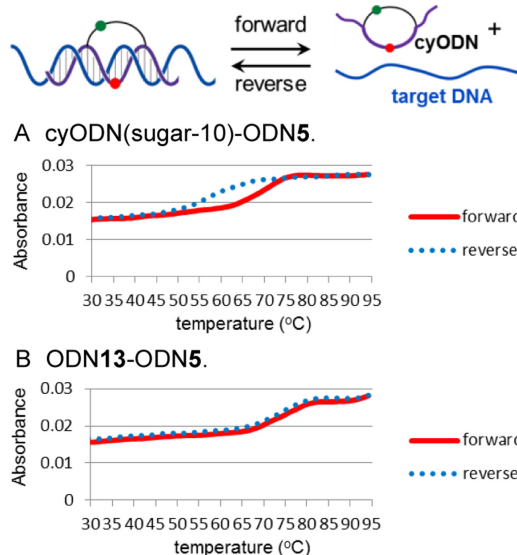
Figure 8. T_m curves with (**A**) cyODN(sugar-10)-ODN**5**, (**B**) ODN**13**-ODN**5**. The forward and reverse T_m curves are shown as a red solid line and blue dotted line, respectively.

ORN, a slight entropic stabilization was observed (Tables 9 and 10). In contrast, as for the pseudorotaxane of cyODN(sugar)-ODN and cyODN(base)-ORN, the $\Delta S_{off}^{\ddagger}$ value increased as the ring size decreased probably due to the effect of other factors. Especially, since the pseudorotaxane of cyODN(sugar-13)-ODN had an extremely low en-

thalpy and entropy of activation, we considered that this complex was intrinsically strained.

Thermo-reversible pseudorotaxane formation

Based on the results of the pseudorotaxane formation and dissociation, the thermo-reversible pseudorotaxane formation was performed using cyODN(sugar-13) with the highest formation rate. The pseudorotaxane formation and dissociation were carried out by a 5-min heating at 50°C and 80°C, respectively. The formation yields of the DNA target ODN**5** were >93%, in contrast, after the dissociation step, the ratios of the pseudorotaxane were <4%, indicating the clear thermo-reversibility of the cyODN for the pseudorotaxane formation (Figure 10). The same thermo-reversibility was observed using the RNA target ORN**1** (Supplementary Figure S5). This thermo-reversibility will be useful for capturing and releasing a small target nucleic acid such as the miRNA and dynamic DNA/RNA nanotechnology.

CONCLUSION

We have described the slippage mechanism of the double-tailed cyODN via the non-threaded structure by the hybridization of the tail parts. The non-threaded structure formation would guide the threading by efficiently approaching the ring part to the end of the target. However, the strong hybridization of the tail parts also caused decelerating of the threading step because one tail part had to dissociate from the target for the threading. Since cyODN(sugar-13) com-
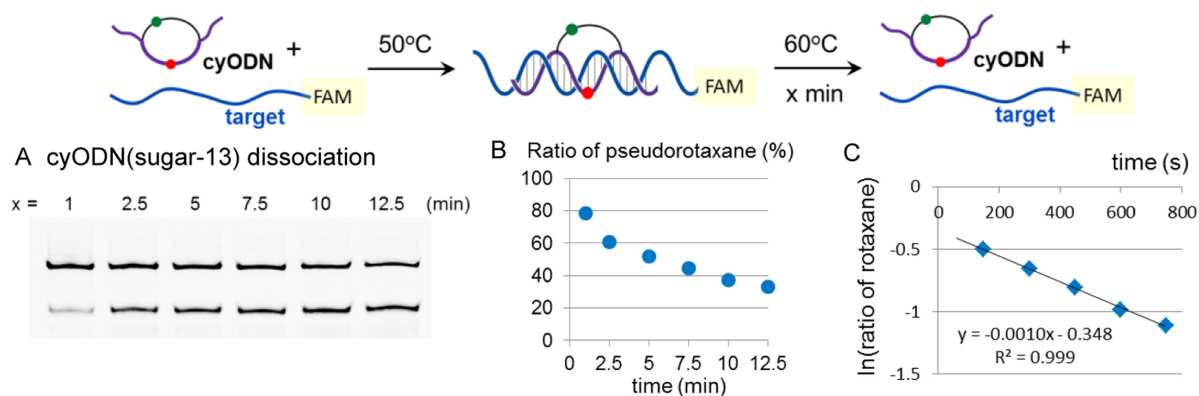
Figure 9. Determination of dissociation rate constants (k_{off}) of cyODNs. First, the pseudorotaxane structure was formed with cyODN (0.6 μM) and target ODN**5** (0.4 μM) in phosphate buffer (20 mM, pH 7.2) containing NaCl (100 mM) at 50°C for 15 min. The dissociation of cyODN was then performed with the pseudorotaxane (0.1 μM) and non-labeled target ODN**14** (2 μM) in the same buffer at 60°C. (**A**) Gel image of cyODN(sugar-13) dissociation. (**B**) Ratio of pseudorotaxane. (**C**) Calculation of the first-order rate constant (k_{off}) of cyODN(sugar-13) dissociation.

Table 9. The dissociation rate constants (k_{off}) and the activation parameters for the dethreading from DNA template

cyODN	k_{off} [s^{-1}] (60°C)	$\Delta G_{off}^{\ddagger}$ [kJmol^{-1}] (60°C)	$\Delta H_{off}^{\ddagger}$ [kJmol^{-1}]	$\Delta S_{off}^{\ddagger}$ [Jmol^{-1}K^{-1}]
Base-10	8.0×10^{-4}	70	3.6×10^2	8.6×10^2
Base-11	1.5×10^{-3}	68	3.7×10^2	9.2×10^2
Base-13	$2,2 \times 10^{-3}$	67	4.7×10^2	12.2×10^2
Sugar-10	7.3×10^{-5}	76	4.3×10^2	10.5×10^2
Sugar-11	2.3×10^{-4}	73	4.0×10^2	9.7×10^2
Sugar-13	1.2×10^{-3}	68	3.0×10^2	7.0×10^2

Table 10. The dissociation rate constants (k_{off}) and the activation parameters for the dethreading from RNA template

cyODN	k_{off} [s^{-1}] (67.5°C)	$\Delta G_{off}^{\ddagger}$ [kJmol^{-1}] (67.5°C)	$\Delta H_{off}^{\ddagger}$ [kJmol^{-1}]	$\Delta S_{off}^{\ddagger}$ [Jmol^{-1}K^{-1}]
Base-10	1.1×10^{-2}	63	5.3×10^2	13.6×10^2
Base-11	1.3×10^{-2}	63	4.9×10^2	12.4×10^2
Sugar-10	1.4×10^{-4}	76	3.8×10^2	8.8×10^2
Sugar-11	2.0×10^{-4}	75	3.9×10^2	9.4×10^2
Sugar-13	1.9×10^{-4}	75	4.0×10^2	9.4×10^2
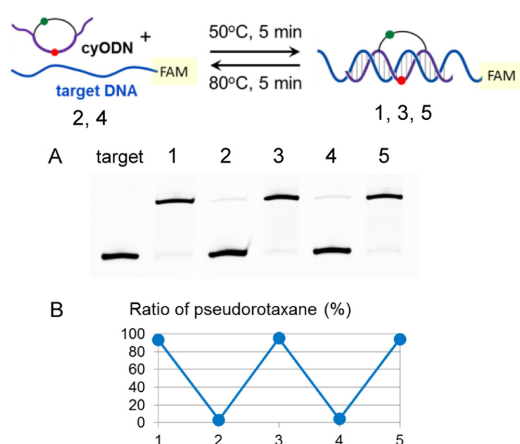
Figure 10. Thermo-reversible pseudorotaxane formation using cyODN(sugar-13). The formation was carried out with cyODN(sugar-13) (0.5 μM) and target ODN**5** (0.25 μM) in phosphate buffer (20 mM, pH 7.2) containing NaCl (100 mM) at 50°C for 5 min and the dissociation was carried out at 80°C for 5 min. (**A**) Gel image of thermoreversible pseudorotaxane formation. (**B**) The abundance ratio of pseudorotaxane.

prehensively has the best tail combination of the six synthesized cyODNs, the formation rate would be remarkably high. Based on the proposed mechanism, developing the cyODN with a higher pseudorotaxane formation rate will be possible by modulating the stability of the tail parts.

We have also shown the thermal and kinetic stabilities of the pseudorotaxanes. The pseudorotaxanes showed interesting characteristics unlike the canonical duplex such as the hysteresis loop in the T_m measurements and the kinetic stabilization by lengthening the target. Using the properties of both the pseudortotaxane formation and dissociation, the thermo-reversible pseudorotaxane formation has been demonstrated with the cyODN(sugar-13) for the study of a small nucleic acid such as miRNA. If the photo-response moiety, such as azobenzene derivatives (25,26), is incorporated into the cyODN, the photo-reversible pseudorotaxane formation could be possible and will be a useful tool for dynamic DNA/RNA nanotechnology.

Recently, many endogenous circular RNAs have been identified and the new functions have been characterized. One of the exciting findings is that the circular RNAs could function as miRNA sponges (27,28). Although the circular RNAs are extremely large, the complex with miRNAs

should be a threaded structure. Given that the functions of many endogenous circular RNAs will still remain unknown, the threaded structure, such as the pseudorotaxane, might exist in many organisms. The proposed mechanism of the pseudorotaxane formation with the double-tailed cyODN and the properties of the cyODNs and the pseudorotaxane structures could be a catalyst to find new functions of circular nucleic acids and elucidate the threading mechanism regarding other small synthetic molecules and biopolymers.

SUPPLEMENTARY DATA

Supplementary Data are available at NAR Online.

FUNDING

REFERENCES

1. Mohsen,M.G. and Kool,E.T. (2016) The discovery of rolling circle amplification and rolling circle transcription. *Acc. Chem. Res.*, **49**, 2540–2550.
2. Ali,M.M., Li,F., Zhang,Z., Zhang,K., Kang,D.K., Ankrum,J.A., Le,X.C. and Zhao,W. (2014) Rolling circle amplification: a versatile tool for chemical biology, materials science and medicine. *Chem. Soc. Rev.*, **43**, 3324–3341.
3. Abe,N., Hiroshima,M., Maruyama,H., Nakashima,Y., Nakano,Y., Matsuda,A., Sako,Y., Ito,Y. and Abe,H. (2013) Rolling circle amplification in a prokaryotic translation system using small circular RNA. *Angew. Chem. Int. Ed.*, **52**, 7004–7008.
4. Abe,N., Matsumoto,K., Nishihara,M., Nakano,Y., Shibata,A., Maruyama,H., Shuto,S., Matsuda,A., Yoshida,M., Ito,Y. *et al.* (2015) Rolling circle translation of circular RNA in living human cells. *Sci. Rep.*, **5**, 16435.
5. Clusel,C., Ugarte,E., Enjolras,N., Vasseur,M. and Blumenfeld,M. (1993) Ex vivo regulation of specific gene expression by nanomolar concentration of double-stranded dumbbell oligonucleotides. *Nucleic Acids Res.*, **21**, 3405–3411.
6. Hosoya,T., Takeuchi,H., Kanesaka,Y., Yamakawa,H., Miyano-Kurosaki,N., Takai,K., Yamamoto,N. and Takaku,H. (1999) Sequence-specific inhibition of a transcription factor by circular dumbbell DNA oligonucleotides. *FEBS Lett.*, **461**, 136–140.
7. Abe,N., Abe,H. and Ito,Y. (2007) Dumbbell-shaped nanocircular RNAs for RNA interference. *J. Am. Chem. Soc.*, **129**, 15108–15109.
8. Abe,N., Abe,H., Nagai,C., Harada,M., Hatakeyama,H., Harashima,H., Ohshiro,T., Nishihara,M., Furukawa,K., Maeda,M. *et al.* (2011) Synthesis, structure, and biological activity of dumbbell-shaped nanocircular RNAs for RNA interference. *Bioconjug. Chem.*, **22**, 2082–2092.
9. Wu,L., Wang,Y., Wu,J., Lv,C., Wang,J. and Tang,X. (2013) Caged circular antisense oligonucleotides for photomodulation of RNA digestion and gene expression in cells. *Nucleic Acids Res.*, **41**, 677–686.
10. Seyfried,P., Eiden,L., Grebenovsky,N., Mayer,G. and Heckel,A. (2017) Photo-tethers for the (Multi-)Cyclic, conformational caging of long oligonucleotides. *Angew. Chem. Int. Ed.*, **56**, 359–363.
11. Yamazoe,S., Liu,Q., McQuade,L.E., Deiters,A. and Chen,J.K. (2014) Sequential gene silencing using wavelength-selective caged morpholino oligonucleotides. *Angew. Chem. Int. Ed.*, **53**, 10114–10118.
12. Kool,E.T. (1998) Recognition of DNA, RNA, and proteins by circular oligonucleotides. *Acc. Chem. Res.*, **31**, 502–510.
13. Jester,S.S. and Famulok,M. (2014) Mechanically interlocked DNA nanostructures for functional devices. *Acc. Chem. Res.*, **47**, 1700–1709.
14. Lu,C.H., Cecconello,A. and Willner,I. (2016) Recent advances in the synthesis and functions of reconfigurable interlocked DNA nanostructures. *J. Am. Chem. Soc.*, **138**, 5172–5185.
15. Liu,Y., Kuzuya,A., Sha,R., Guillaume,J., Wang,R., Canary,J.W. and Seeman,N.C. (2008) Coupling across a DNA helical turn yields a hybrid DNA/organic catenane doubly tailed with functional termini. *J. Am. Chem. Soc.*, **130**, 10882–10883.
16. Onizuka,K., Nagatsugi,F., Ito,Y. and Abe,H. (2014) Automatic pseudorotaxane formation targeting on nucleic acids using a pair of reactive oligodeoxynucleotides. *J. Am. Chem. Soc.*, **136**, 7201–7204.
17. Erbas-Cakmak,S., Leigh,D.A., McTernan,C.T. and Nussbaumer,A.L. (2015) Artificial Molecular Machines. *Chem. Rev.*, **115**, 10081–10206.
18. Deutman,A.B., Monnereau,C., Elemans,J.A., Ercolani,G., Nolte,R.J. and Rowan,A.E. (2008) Mechanism of threading a polymer through a macrocyclic ring. *Science*, **322**, 1668–1671.
19. Deutman,A.B., Varghese,S., Moalin,M., Elemans,J.A., Rowan,A.E. and Nolte,R.J. (2015) Slippage of a porphyrin macrocycle over threads of varying bulkiness: implications for the mechanism of threading polymers through a macrocyclic ring. *Chem. Eur. J.*, **21**, 360–370.
20. Dommerholt,J., Schmidt,S., Temming,R., Hendriks,L.J., Rutjes,F.P., van Hest,J.C., Lefeber,D.J., Friedl,P. and van Delft,F.L. (2010) Readily accessible bicyclononynes for bioorthogonal labeling and three-dimensional imaging of living cells. *Angew. Chem. Int. Ed.*, **49**, 9422–9425.
21. Asakawa,M., Ashton,P.R., Ballardini,R., Balzani,V., Bělohradský,M., Gandolfi,M.T., Kocian,O., Prodi,L., Raymo,F.M., Stoddart,J.F. *et al.* (1997) The slipping approach to self-assembling [n]rotaxanes. *J. Am. Chem. Soc.*, **119**, 302–310.
22. Huang,X., Huang,S., Zhai,B., Zhang,Y., Xu,Y. and Wang,Q. (2012) Slipping synthesis of cucurbit[7]uril-based [2]rotaxane in organic environment. *Tetrahedron Lett.*, **53**, 6414–6417.
23. Meek,S.J., Pitman,C.L. and Miller,A.J.M. (2016) Deducing reaction mechanism: a guide for students, researchers, and instructors. *J. Chem. Educ.*, **93**, 275–286.
24. Sugimoto,N., Nakano,S., Yoneyama,M. and Honda,K. (1996) Improved thermodynamic parameters and helix initiation factor to predict stability of DNA duplexes. *Nucleic Acids Res.*, **24**, 4501–4505.
25. Kamiya,Y. and Asanuma,H. (2014) Light-driven DNA nanomachine with a photoresponsive molecular engine. *Acc. Chem. Res.*, **47**, 1663–1672.
26. Lohmann,F., Ackermann,D. and Famulok,M. (2012) Reversible light switch for macrocycle mobility in a DNA rotaxane. *J. Am. Chem. Soc.*, **134**, 11884–11887.
27. Memczak,S., Jens,M., Elefsinioti,A., Torti,F., Krueger,J., Rybak,A., Maier,L., Mackowiak,S.D., Gregersen,L.H., Munschauer,M. *et al.* (2013) Circular RNAs are a large class of animal RNAs with regulatory potency. *Nature*, **495**, 333–338.
28. Hansen,T.B., Jensen,T.I., Clausen,B.H., Bramsen,J.B., Finsen,B., Damgaard,C.K. and Kjems,J. (2013) Natural RNA circles function as efficient microRNA sponges. *Nature*, **495**, 384–388.